Chemical Engineering Journal 458 (2023) 141383

Contents lists available at ScienceDirect

Chemical Engineering Journal

journal homepage: www.elsevier.com/locate/cej

Dual-functional vinylpyrrolidone electrolyte additive as anode surface leveler and cathode catalyst for lithium Metal-Oxygen batteries

Jun-Seo Lee [a], Kihyun Shin [b,c], Seo-Young Jun [a], Suji Kim [a], Won-Hee Ryu [a,d,*]

[a] Department of Chemical and Biological Engineering, Sookmyung Women's University, 100 Cheongpa-ro 47-gil, Yongsan-gu, Seoul 04310, Republic of Korea
[b] Department of Chemistry and the Oden Institute of Computational Engineering and Sciences, University of Texas at Austin, 100 E 24th Street A5300, Austin TX78712, USA
[c] Department of Materials Science and Engineering, Hanbat National University, 125 Dongseo-daero, Yuseong-gu, Daejeon 34158, Republic of Korea
[d] Institute of Advanced Materials and Systems, Sookmyung Women's University, 100 Cheongpa-ro 47-gil, Yongsan-gu, Seoul 04310, Republic of Korea

ARTICLE INFO

Keywords:
1-vinyl-2-pyrrolidone
Bifunctional additive
Leveler
Lithium metal anode
Catalyst
Lithium-oxygen battery

ABSTRACT

To overcome the limitations of lithium-ion batteries, Li metal–O_2 breathing batteries (LMOBs) have been extensively investigated because of the exceptional energy density provided by the O_2 cathode and Li metal anode. However, the dendrite growth and consequent surface degradation on the Li metal anode are significant issues prohibiting the safe and long-term cell operation. In this study, vinylpyrrolidone (VP) was homogeneously introduced into the electrolyte of LMOBs to flatten the Li metal anode and eliminate the dendrite growth and to activate a cathodic reaction with reduced overpotential. A smooth surface morphology and high-quality solid-electrolyte interface layer were achieved on the Li metal anode owing to dipolar VP molecules. We also verified the catalytic effect of VP molecules on the O_2 cathode reaction. Finding a homogeneous and dual-function electrolyte additive to stabilize the Li metal anode and activate the Li-O_2 cathode reaction is a new strategy to develop tailored LMOBs.

1. Introduction

Because of the widespread use of smart wireless devices and electric vehicles, the demand for batteries as standalone electric power supplies and energy storage devices has extensively increased [1,2]. The Li-ion batteries used for commercial energy storage must surpass their theoretical energy density limitation to satisfy the needs of the growing battery market [3]. Efforts have been devoted to explore alternative cathode and anode components to enable a high capacity and corresponding energy density [4–6]. A Li metal anode can offer a considerably higher theoretical specific capacity than a conventional graphite anode (graphite: 370 mAh g^{-1}; Li metal: 3800 mAh g^{-1}) and the lowest reduction potential (-3.040 V vs the standard hydrogen electrode), which have attracted significant attention [7,8]. Despite the energy merit of Li metal anodes, issues have hindered their application as potential alternatives for commercialized graphite anodes. First, Li metal anodes induce unwanted side reactions with electrolytes because of their high reactivity, which originates from a low 1st ionization energy (520 kJ mol^{-1}). In addition, inhomogeneous morphological deposition (dendrite growth) easily occurs on the Li metal anode surface during repeated cell operation, resulting in a sudden electrical short and unavoidable safety concerns [9,10]. Because dendrite growth is fatal, especially at a high charge current density, it is necessary to address the paradoxical demand to develop a fast-charging battery system for large-capacity smart devices and electric vehicles. In this regard, relevant studies have demonstrated various methods to eliminate the issues by (i) introducing conductive support, such as a three-dimensional interlayer structure, (ii) uniformly distributing an electric flux on a current collector, (iii) adding functional additives, or (iv) coating the lithium anode surface forming protection layer [11–21].

To construct a cell with a Li metal anode as a counter electrode, Li-less and transition metal (M)-less cathode materials, such as oxygen (O_2), carbon dioxide (CO_2), or sulfur (S) cathodes, have been considered because of their exceptionally high energy densities (Li-O_2: ~3500 Wh kg^{-1}; Li-CO_2: ~1876 Wh kg^{-1}Li-S: ~2600 Wh kg^{-1}) compared to that of lithium-ion batteries [22–24]. As an ideal combination with Li metal anodes to achieve a high energy density, Li-O_2 batteries have shown attractive characteristics because (i) their cathode sources use abundant

* Corresponding author at: Department of Chemical and Biological Engineering, Sookmyung Women's University, 100 Cheongpa-ro 47-gil, Yongsan-gu, Seoul 04310, Republic of Korea.
E-mail address: whryu@sookmyung.ac.kr (W.-H. Ryu).

https://doi.org/10.1016/j.cej.2023.141383
Received 17 October 2022; Received in revised form 27 November 2022; Accepted 7 January 2023
Available online 9 January 2023

and lightweight O_2 instead of a heavy metal component; (ii) they produce multi-electron reactions (more than 2) corresponding to a high capacity; (iii) there is an infinite O_2 supply from the atmosphere; (iv) they have a high operating redox voltage of 2.98 V [24,25]. The reversible formation and decomposition reactions of lithium oxides ($xLi^+ + O_2$ (gas) + $xe^- \leftrightarrow Li_xO_2$ (solid), where x = 1 or 2, E^o = 2.96 V vs Li/Li^+) occur on the oxygen electrode surface during the discharge and charge operations [26]. However, Li-O_2 cells have large overpotential and poor reversibility, which originate from the difficult decomposition of the solid Li_xO_2 insulating phase during charging. Therefore, the introduction of oxygen evolution reaction (OER) and oxygen reduction reaction (ORR) catalysts is required [25,27–29]. While the performance of Li-O_2 cells can be improved by decorating the electrode with a solid catalyst (e.g., Pt, Pd, or Au), it is eventually deactivated by the accumulation of Li_xO_2 products as the cycle progresses [30–32]. Therefore, soluble and accessible catalysts called redox mediators (RMs) have been directly introduced into the electrolyte as an alternative catalyzing strategy, regardless of the limiting catalyst deactivation. These RMs are oxidized by the charge instead of the discharge products. Thereafter, the RMs chemically oxidize and decompose the Li_xO_2 products via a subsequent reduction and restoration to the original state. Possible RM candidates, such as Li iodide, Li bromide, metal phthalocyanines, heme, and polyoxometalates have been studied to enhance the Li-O_2 cell performance [33–37]. From state-of-the-art research, porphyrin structured molecules are also noted as RMs directly interacting with superoxide species [38,39]. However, the RMs diffused to Li anodes tended to irreversibly degrade the Li metal anodes as an unexpected side reaction [40,41]. Therefore, a suitable electrolyte additive, such as an RM, should satisfy the strict requirements for high-performance batteries, and the development of a dual-function additive that both stabilizes the Li metal anode and activates the cathode reaction is ultimately needed.

In this study, we introduced dipolar vinylpyrrolidone (VP) as a novel electrolyte additive that simultaneously functioned as a Li anode surface leveler and soluble cathode catalyst for high-performance Li metal–O_2 breathing batteries (LMOBs). Li^+ ion deposition in the battery system occurs via an electroplating process wherein the metal is reduced by an electromotive force at the electrochemical double layer. We employed this electroplating additive technique and evaluated VP-based surface leveler candidates for electroplating. Leveler additives possessing a permanent dipole moment are typically known to effectively prevent inhomogeneous dendrite growth on the electrode surface during electroplating by sticking on localized high current spots and subsequently slowing down the over-plating [42–44]. Through calculations using the GaussView 6 program, we confirmed the dipole moment and polarizability of the VP molecule, which showed its ability to level the surface of the Li metal anode. Significantly, it was also effective at facilitating the decomposition of Li_xO_2 products because the oxygen in the VP could selectively attract Li^+ ions, which have a positive charge in Li_2O_2 (Fig. 1), demonstrating the bi-functional property of the VP additive for electrochemical reactions on both the anode and cathode. We investigated the surface leveling effects of the VP additive in Li-Li symmetric cells using electrochemical tests and *ex-situ* characterizations. We used density functional theory (DFT) calculations to determine the binding energy of Li and VP to analyze the effect of VP on dendrite suppression and surface reconstruction. Furthermore, Li-O_2 cells with the VP additive were evaluated to confirm the catalytic effects for the OER. Considering the dipolar properties of electroplating additives, our research strategy could provide fresh insights and inspiration regarding the versatile utilization of classical electroplating techniques to realize next-generation Li metal batteries or LMOBs.

2. Result and discussion

2.1. Li-Li symmetric cells employing VP additive

The electron localization on defect or nodule spots, especially for a highly applied current reaction, such as fast charging, unexpectedly induces non-homogeneous Li nucleation and consequent dendrite growth, resulting in reaction instability and a short in the cell [45]. A localized electron distribution originating from a partially coordinated oxygen and vinyl group in a pentagonal pyrrolidone structure produces a dipole moment (3.54 D), allowing facile adsorption on the charged Li metal anode (Fig. 1). Further, the substantial polarizability value (58.2 A.U.) of the VP molecules corresponding to the charge localization ability accelerates the surface interaction on the charged electrode. In this regard, the homogeneous nucleation and uniform growth of Li can be achieved by introducing the VP molecule as an electroplating surface leveler in the electrolyte. To verify the surface leveling effect of VP on a Li metal anode, electrochemical tests were conducted using Li-Li symmetric cells with the VP additive in the electrolyte (Fig. 2). Such a Li-Li symmetric cell system has been considered to demonstrate the electrochemical performances of Li metal electrodes in most studies because it represents the Li stripping/plating mechanism in Li metal batteries. Since VP is a monomer that forms PVP in the form of a polymer, the optimal length of the VP additive is evaluated through cell test. As a result, only the VP monomer showed improved cycle performance

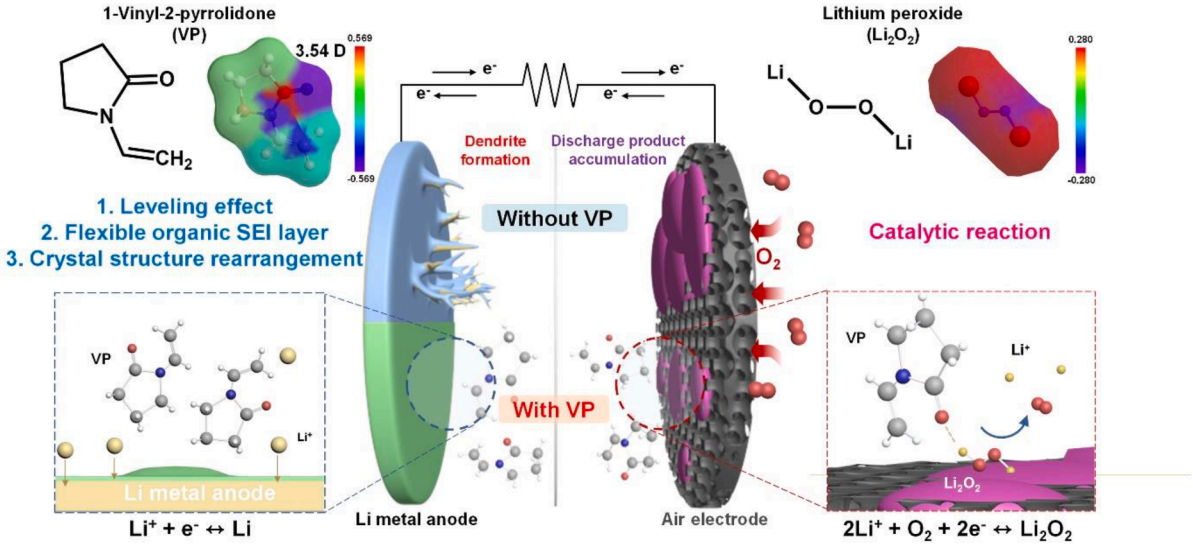

Fig. 1. Schematic illustration of the VP molecule as a dual-functional electrolyte additive affecting both the anode and cathode in a LMOB system.

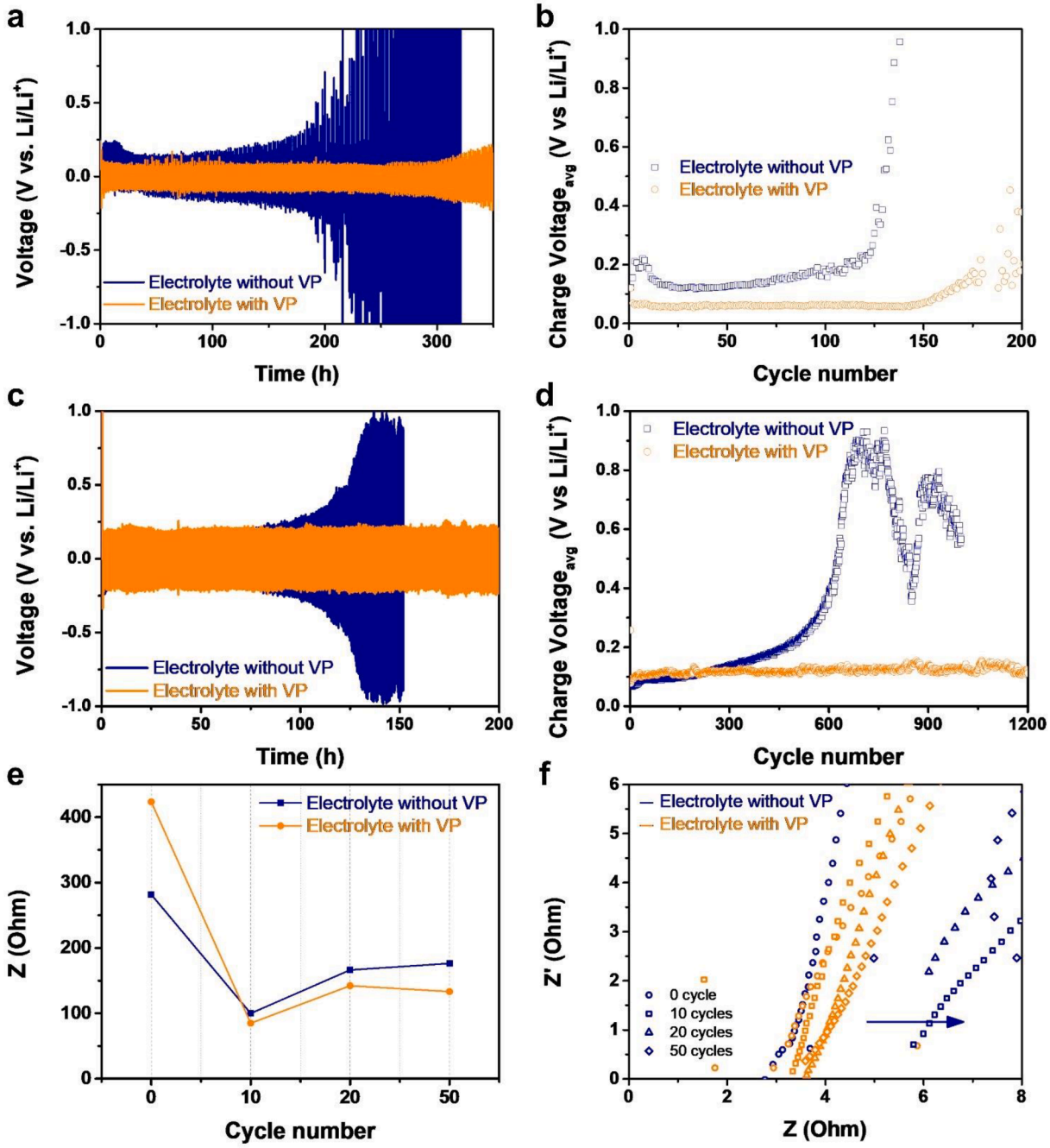

Fig. 2. Li-Li symmetric cell tests in VP containing electrolyte Cell performance tests of the Li metal electrodes with plating capacity of 1 mAh cm^{-2} at a low current density of 1 mA cm^{-2} depicted as (a) charge/discharge curve and (b) average charge voltage and at a high current density of 10 mA cm^{-2} depicted as (c) charge/discharge curve and (d) average charge voltage. (e) Charge transfer resistance from Nyquist plot of both cells using the pristine electrolyte and electrolyte with VP at different cycle number and (f) ohmic resistances from the magnified Nyquist plots.

compared to the cell without additive (Fig. S1). By simply introducing the VP molecule in the Li-Li symmetric cell, we achieved a significantly improved cycling performance with a reduced and stabilized overpotential over 300 h compared to that of a pristine cell (Fig. 2**a**). The charging voltage of a Li-Li symmetric cell without VP substantially increased after 100 cycles (Fig. 2**b**). In contrast, the cell that contained VP stably maintained a low voltage value even after 150 cycles. Both the overpotential in the voltage profile and average charge voltage value for cycling were significantly reduced in the case of the VP-containing cells, indicating the stabilizing effect of VP for Li metal anodes during repeated cycling. The voltage increase at the end of cycling is associated with dendrite growth because the insulating solid-electrolyte interface (SEI) layers surrounding dead Li particles detached from the Li dendrite substantially accumulated on the anode surface. In previous studies, Li-Li symmetric cells failed as a result of dendrite growth as the number of cycles increased [45,46]. The dendrite form and voltage profile differed depending on the current density and state of the cell. In this study, a moss-like dendrite was formed. Therefore, the electrolyte was consumed because of a continuous increase in dead Li, which caused a rapid increase in the overpotential. When the cells without VP were disassembled, the electrodes and separator were dry, with the entire amount of electrolyte consumed, unlike the cells with VP. This result was consistent with the failure mechanism observed in previous studies.

Therefore, a stable voltage profile for the VP-containing cell implied

that the dendrite growth was effectively suppressed by the surface leveling effects of the VP additive in the electrolyte [47,48]. Because dendrite growth is more severe at a high current density [49], Li-Li symmetric cell failed more quickly due to the fast rate of Li deposition causing non-uniform surface and dendrite growth. (**Fig. S2**) We performed Li-Li symmetric cell tests at a 10-fold higher current density of 10 mA cm^{-2} to confirm that VP also can level the surface of the anode even at high current density (Fig. 2**c and d**). At the high current density, the driving force for Li^+ ion deposition becomes high, which rendered it relatively more vulnerable to dendrite growth. VP-containing cell showed considerably more stabilizing effects at a high current density, compared to the pristine cell without VP. Even though the Li-Li symmetric cell without VP showed a substantial overpotential increase after approximately 100 h, the cell containing electrolyte with VP showed a constant average charge voltage even after 200 h (Fig. 2**c**). The voltage profiles of the Li-Li symmetric cells showed that the VP effectively suppressed the dendrite growth on the Li metal anode. At 1 mA cm^{-2}, the cyclability improved by approximately 1.5 times when the VP was added, but at 10 mA cm^{-2}, the cyclability increased more than two times, and a relatively stable overpotential was observed. The charging voltage of the Li-Li symmetric cell without VP showed an increase at the start of the cycle test (Fig. 2**d**). In contrast, the cell containing VP showed a stable voltage profile without a voltage increase for up to 1200 cycles. This result verified that the VP effectively inhibited the dendrite growth and prevented cell degradation even under high current density conditions.

Although the VP additive effectively stabilized the Li anode through the leveling effect and reduced the cell overpotential, the VP molecules could interrupt the Li-ion transfer via surface adsorption on the electrochemical interface between the electrolyte and Li metal anode and consequently hinder the charge transfer reaction. VP has negatively charged functional groups (oxygen and vinyl groups), with a permanent dipole moment in the molecular structure (Fig. 1). Electrochemical impedance spectroscopy (EIS) profiles were obtained at different cycles to elucidate the degree of charge transfer hindrance by the VP molecules (Fig. 2**e and f**). The Nyquist plot at low frequencies is associated with the charge transfer resistance at the Li-anode/electrolyte interface (**Fig. S3a**). Prior to the cell operation, the pristine cell without VP showed a relatively lower charge transfer resistance (~280 Ω) compared to the VP-containing cell (~430 Ω) because of the surface adsorption of VP on the electrode. During cycling, the charge transfer resistance first decreased and then increased continuously after the 20th cycle for pristine cells. In contrast, the charge transfer resistance of the VP-containing cell did not increase after the 20th cycle. After the 50th cycle, the VP-containing cell exhibited an even lower charge transfer resistance with a difference of approximately 50 Ω compared to that of the pristine cell without VP. To examine the ohmic resistance of the cell, we present the left x-intercept of the Nyquist plot, which is associated with the ohmic resistance of the Li-Li symmetric cell (Fig. 2**f**). The ohmic resistance includes the values for the electrolyte, separator, and electrodes, which are significantly related to the state of cell [50,51]. Although the ohmic resistance increased for the pristine cell during cycling, a cell containing the electrolyte with VP showed an approximately constant resistance even after 50 cycles. According to the equivalent circuit model (**Fig. S3b**), the ohmic resistance is due to dendrite growth during Li stripping /deposition. In the absence of VP, the growth of dendrite results in increased ohmic resistance after cycles. In addition, the charge transfer resistance, which gradually increased over the cycle, was caused by contact resistance from dead Li which were detached from Li metal surface during the stripping process of grown dendrite.

2.2. Morphological surface leveling effect of the VP additive

To investigate the morphological evolution of the lithium anode surface for the cell reaction, we obtained SEM images after 1000 cycles of the charge/discharge test (Fig. 3**a–f**). The Li metal anode operated in the electrolyte without VP had a dark, rough appearance after disassembling the coin-type cell (Fig. 3**g**). A vertical image (Fig. 3**c**) showed that the entire surface was full of dendrite structures and covered with bumpy passivate layers. In contrast, the Li metal anode operated with VP in the electrolyte showed a flat surface with high optical reflectivity even after 1000 cycles (Fig. 3**h**). The surface morphology of the Li anode cycled with the VP additive showed no significant curvature on the surface except negligible and unavoidable passivation at the center. The result regarding the apparent morphological difference verified the surface leveling effects of the VP additive during repeated Li deposition/stripping processes. Cross-sectional observations of the cycled Li anode confirmed a smooth feature along the vertical direction of the anode, unlike the pristine one (Fig. 3**f**). The passivation layer located at the center of the electrode was estimated to be a lithium hydroxide layer, which was formed through the electrolyte (tetraethylene glycol dimethyl ether, TEGDME) decomposition [52]. To evaluate the roughness and surface structure more precisely, we also obtained atomic force microscopy (AFM) images in a glove box. Similar to the SEM images, the surface roughness was much higher in the absence of the VP additive than in the case with the VP additive (Fig. 3**i** and **j**) (roughness: 123.68 nm). We could also observe a relatively flat, single structured surface in the presence of the VP additive (roughness: 38.99 nm). These observations confirmed that in the presence of the additive, the dendrite growth was strongly inhibited, and the Li metal anode was safe even after 1000 cycles.

2.3. DFT calculation of Li metal surface reaction employing the VP additive

We used DFT calculations to evaluate how the VP additive helped suppress the Li dendrite formation in terms of the binding energy and changes in the bond length with the presence of VP. We first calculated the binding energy of the Li and VP additive on the Li metal anode. As shown in Fig. 3**k**, we considered terrace, convex, and concave binding sites as the morphology of the surface. Although Li had a positive binding energy value, VP had negative binding energy regardless of the binding sites, which meant the VP was considerably more easily adsorbed on the Li metal than the Li and preferentially covered all the high energy sites (e.g., defects and steps). In other words, during the Li deposition, the VP was effectively adsorbed on a nodule or defect site, causing the leveling effect.

Furthermore, we compared the bond length changes between the Li on the surface and the adsorbate Li next to the VP in each binding site in relation to the presence or absence of the VP molecule (Fig. 3**l**). In the presence of the VP additive, the Li-Li bond length was elongated to approximately 0.08–0.26 Å from the surface. The VP pulled the bonded Li on the surface to further facilitate Li deposition and weakened the binding of surface Li-Li, causing Li diffusion on the surface. Through this Li diffusion, the VP additive facilitated surface reconstruction, leading to flat plating on the surface. These DFT calculation results were identical to our postulation that the VP could act as a leveler not only during the electrodeposition but also in the Li-O_2 battery system.

2.4. Structural growth characteristics and SEI components

To further examine how the crystalline feature of the Li metal anode was affected by the VP additive, Fig. 4**a** shows X-ray diffraction (XRD) results for the Li metal electrode collected after the 10th charge cycle with and without VP additive. There were two main peaks at 36.2° and 52.2° in the XRD pattern of the pristine Li metal sample, which corresponded to the (1 1 0) and (2 0 0) planes of the cubic Li phase (ICDD no. 01–071-5949), respectively. However, a difference in the relative peak intensities was observed between the Li metals cycled with and without the VP additive after 10 cycles. The (2 0 0) peak of the Li metal collected from the cell without VP became stronger than the (1 1 0) peak. In

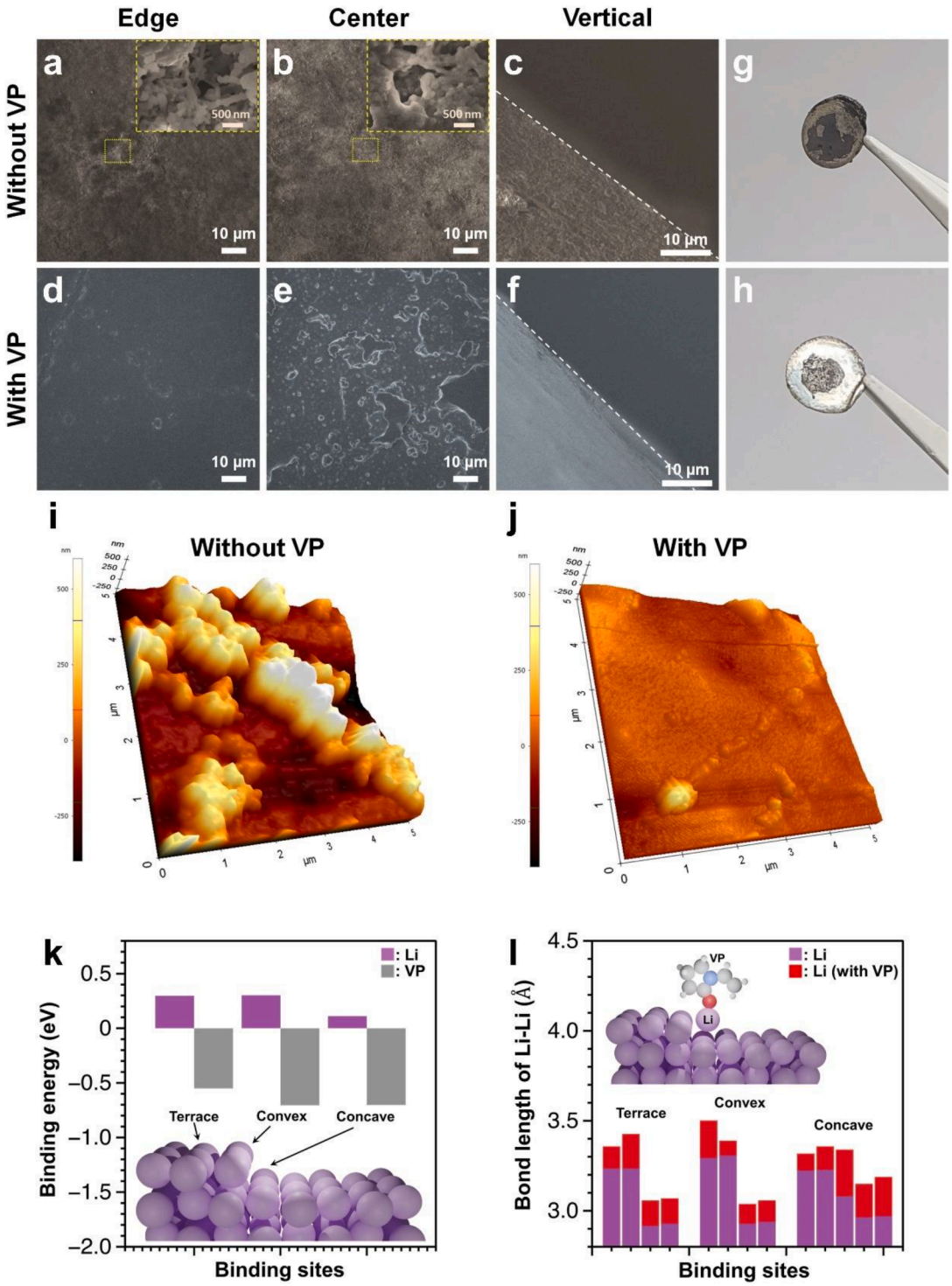

Fig. 3. ***Ex-situ*** **surface morphology characterization of Li-Li symmetric cell at a current density of 10 mA cm^{-2}.** SEM images of the Li metal anode after 1000 cycles of the Li-Li symmetric cell at a current density of 10 mA cm^{-2} in the electrolyte without VP: (**a**) top (edge) (**b**) top (center) (**c**) cross-section and electrolyte with VP: (**d**) top (edge) (**e**) top (center) (**f**) cross-section. Digital pictures of the Li anodes from the disassembled Li-Li symmetric cells: (**g**) without and (**h**) with VP additive. AFM images of the Li metal electrodes after 1000 cycles of the Li-Li symmetric cell at a current density of 10 mA cm^{-2}: (**i**) without VP and (**j**) with VP. DFT calculation results for the (**k**)Li metal anode binding energies of Li and VP on the Li-anode surface with different binding sites: terrace, convex, and concave. (**l**) Bond length comparison between surface Li and adsorbate Li with and without the VP additive.

addition, a LiOH peak was also observed, resulting from electrolyte decomposition, as already shown in previous studies [53]. However, XRD result of the cell with VP additive shows the high relative ratio of the (1 1 0) peak compared to the (2 0 0) peak, with a smaller LiOH peak, indicating that the pristine Li metal structure was successfully preserved by the VP leveler during the Li stripping/plating. The reversible Li deposition and dissolution occurred without unwanted growth in a specific direction, thereby preventing the dendritic growth of Li during cycling. Fig. 4**a** also shows that the VP not only worked as a leveling agent but also prevented the electrolyte decomposition and consequent formation of side products, such as LiOH. To confirm the effect of VP on the crystalline characteristics during stripping and plating of Li-metal,

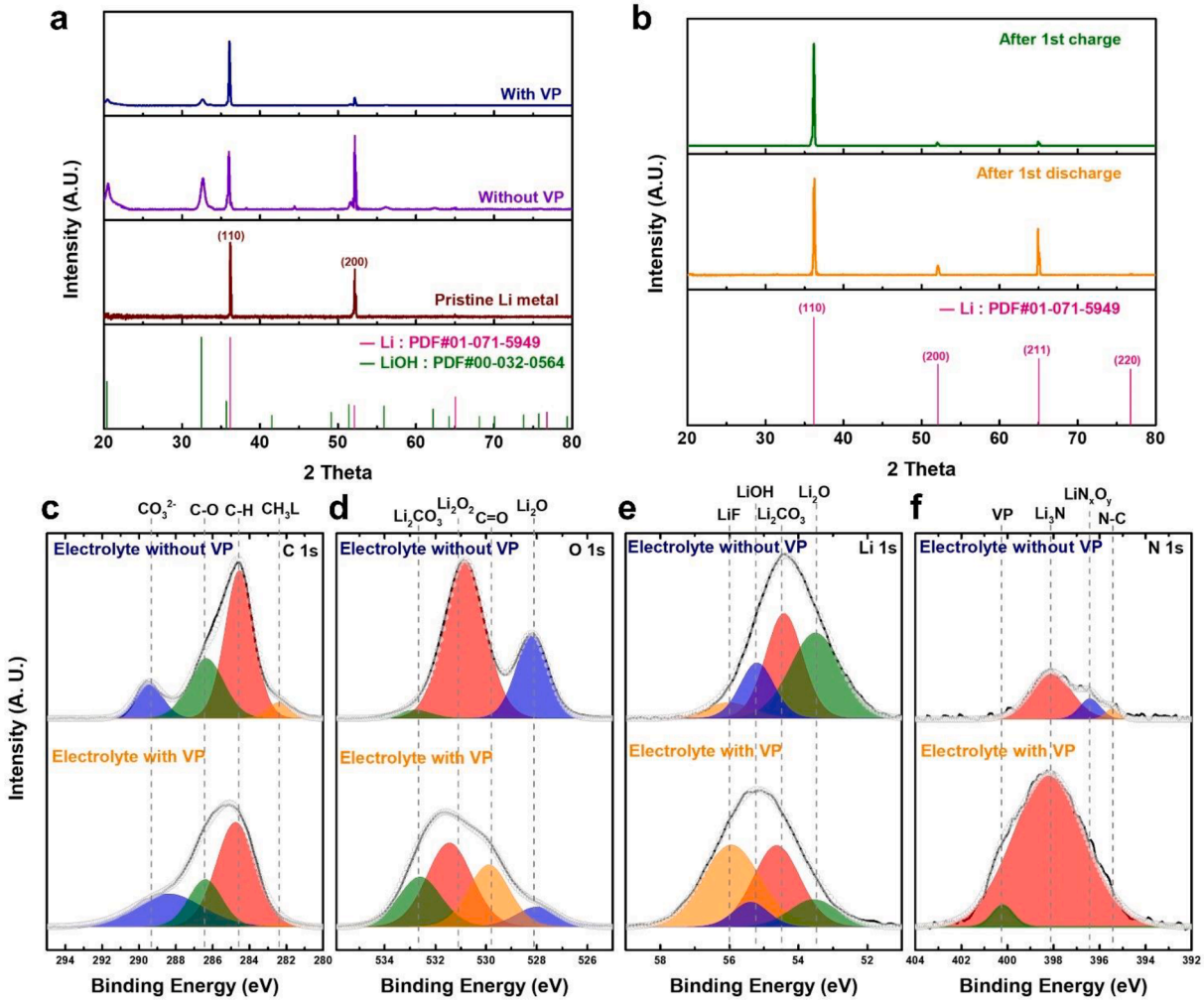

Fig. 4. *Ex-situ* measurements on Li anode. *Ex-situ* X-ray diffraction peaks of Li anode obtained from (**a**) pristine, 10th charged in the electrolyte with and without VP and (**b**) 1st discharged and charged in the electrolyte with VP additive. *Ex-situ* X-ray photoelectron spectra obtained from charged Li anodes in electrolyte with and without VP in (**c**) C 1 s (**d**) O 1 s (**e**) Li 1 s (**f**) N 1 s.

we also acquired XRD patterns of the Li metal anode with the VP additive after the 1st discharge (stripping) and charge (plating) (Fig. 4**b**). Significantly, the (200) peak intensity decreased, and the (211) peak intensity increased after the 1st stripping, and both peaks were marginal after plating. The (110) and (200) planes were actively stripped, and the (110) plane was preferred during plating in the electrolyte with VP. Previous thermodynamic studies demonstrated the rapid nucleation rate of the (110) plane [54]. In addition, the (110) plane exhibited a relatively higher exchange current density than the (200) plane [55]. Lithium was deposited on the (110) plane to create a relatively more homogeneous surface. This also aided in the uniform deposition and stripping of Li with uniform surface energy, which led to a long-term stable Li metal anode. The XRD results corresponded to the SEM morphologies and Li-Li symmetric cell voltage profiles. These results were consistent with previous experimental results that the texturing of the (110) plane due to VP contributed to an increase in the homogeneity of the lithium growth [54]. For further verification of the effect of VP additive, *ex-situ* XRD peaks of Li-anode after discharge of the 50th cycle were compared in presence of VP additive (**Fig. S4**). After the 50th cycle, Li-anode collected from the cell without VP additive showed decreased crystallinity while Li-anode collected from the cell with VP additive showed even more enhanced crystallinity. The VP additive can stabilize and maintain the Li metal during repeated Li stripping and plating as a result of homogeneous Li deposition and diffusion, consistent with DFT calculation results (Fig. 3).

To verify the chemical and crystalline status of the SEI layers on the electrode surface, we performed X-ray photoelectron spectroscopy (XPS) measurements of the electrodes after electroplating and recorded the C 1 s, O 1 s, Li 1 s, and N 1 s spectra (Fig. 4**c–f**). C—O, C—H, and CO_3^{2-} peaks which were related to the SEI layers were found on the surface of the Li electrode. An additional CH_3L peak appeared at 282.4 eV because of the formation of residual side products during electrolyte decomposition. A peak at 289.5 eV related to CO_3^{2-} became considerably stronger and broader in the presence of the VP additive, indicating the dominant existence of lithium carbonate products in the SEI layer species. In the O 1 s spectrum, two main peaks were observed, which corresponded to lithium peroxide and lithium oxide. The Li_2CO_3 and C═O peaks related to carbonate species in the SEI layer were prominent when the VP additive was used, which was consistent with the XPS results for C 1 s. This result implied that oxide-dominant SEI layers were formed in the absence of VP, whereas carbonate-dominant SEI layers were formed in the presence of VP in the electrolyte. By adsorbing on the lithium surface, VP prevented the formation of LiOH side products and accelerated the formation of the carbonate-dominant SEI layer instead of the oxide. An organic carbonate-dominant SEI layer is known to be a stable and flexible passivation layer that prevents side reactions with an electrolyte during cycling. In contrast, an inorganic oxide-dominant SEI layer is relatively stiff and prone to a huge volume change in Li. In the Li 1 s spectrum, a peak for Li_2CO_3 (55 eV) was also found on both electrodes with and without VP. However, peaks related to Li_2O (53.5 eV) and

LiOH (55.2 eV) were mainly observed in the absence of the VP additive, and a LiF peak (56 eV) indicated a fluoride-based carbonate SEI layer in the presence of VP, demonstrating that the VP additive facilitated the formation of a stable and high-quality SEI layer on the Li metal surface, in addition to the expected function of the VP molecule as a surface leveler. The LiF species in the SEI layer formed a lithium protection layer with a low Li diffusion barrier energy, as revealed in other studies [56,57]. In addition, a LiF-based film has strong mechanical properties and substantial electron barrier ability [58]. In the N 1 s spectrum, the Li_3N peak at 398 eV was noticeable for both electrodes. Even in the solution without VP, bis (trifluoromethane) sulfonimide lithium salt (LiTFSI) was ionized, and N- was exposed. Therefore, produced N, Li, and decomposed electrolyte products, lead to increases in the peak intensities of the LiN_xO_y (396.6 eV) and N—C bonds (395.7 eV). In contrast, in the case of a solution containing VP, the VP effectively prevented electrolyte decomposition, and the LiN_xO_y and N—C peaks disappeared. Increased Li_3N peak intensity was observed, indicating a relatively high ion conductivity and the effective inhibition of dendrite lithium formation. The quaternary N peak was also observed at 400.7 eV, which originated from the VP additive [59,60]. Quaternary nitrogen is known to play a role of leveling agents [61,62]. Therefore, the above XPS results demonstrated that the LiF-containing carbonate-based SEI layer that was flexible and advantageous for Li diffusion, not an oxide-based SEI layer, which would easily rupture as a result of a large volume change during a Li deposition/stripping process.

We confirmed that the VP additive effectively offered diverse benefits against the cycling issues with Li metal anodes, including (i) maintaining a flat surface morphology without dendritic growth, (ii)

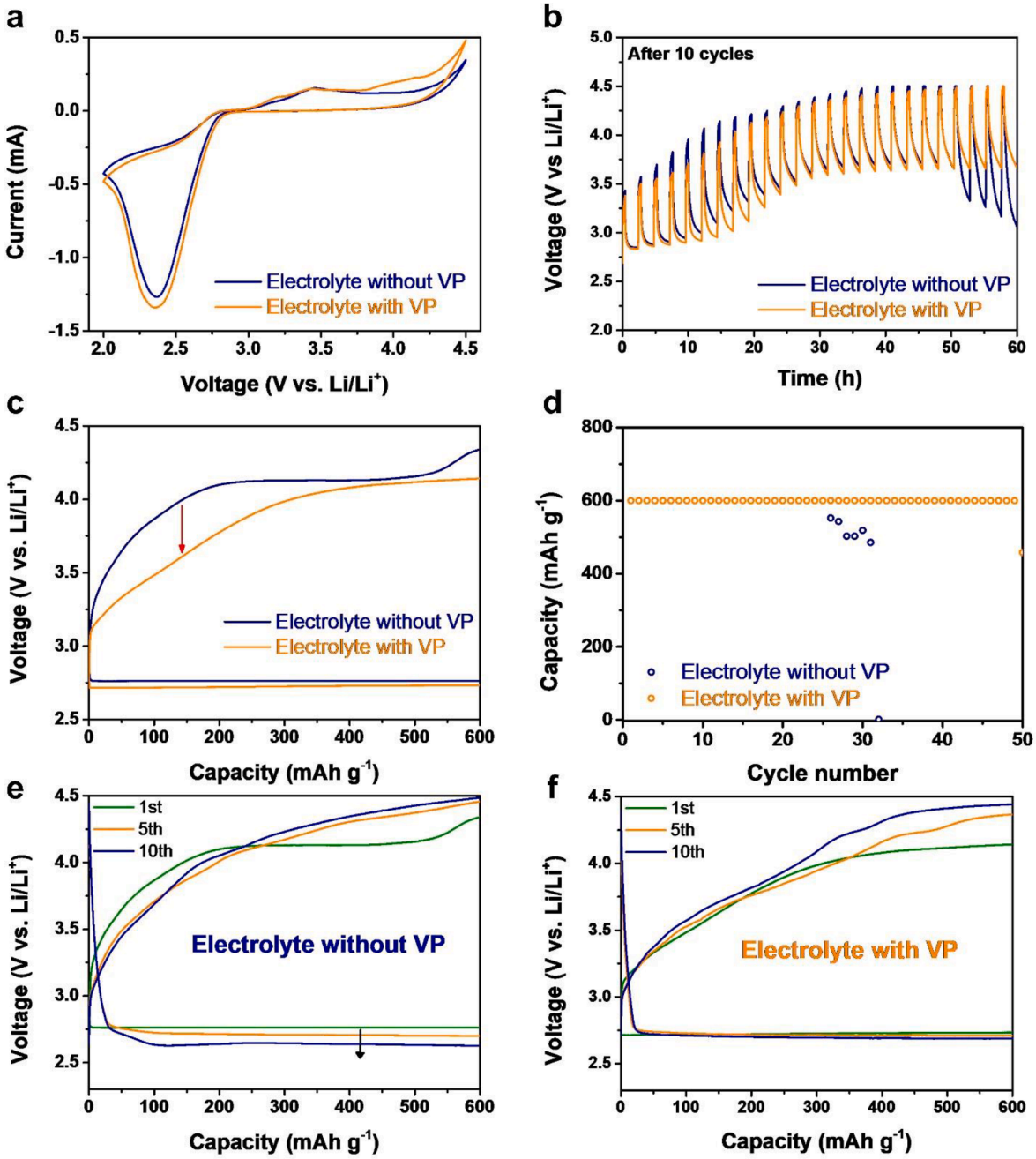

Fig. 5. Electrochemical performance test of Li-O_2 full cell. (a) Cyclic voltammetry curves at a scan rate of 0.1 mV s^{-1} after O_2 purged. (b) Overpotential of Li-O_2 cells obtained by a galvanostatic intermittent titration test (GITT). (c) – (f) Cycle tests performed under a specific capacity limit of 600 mAh g^{-1}_{carbon} in a voltage window between 4.5 and 2.3 V at a current density of 100 mA g^{-1}_{carbon}.

conserving the crystalline orientation of the original Li metal phase indicated with high intensity (1 1 0) peak after cycling, and (iii) forming a high-quality and durable SEI layer film comprising fluoride-based carbonate species. This leads to the successful protection of the Li metal anode and improved safety of the overall cell, even at a high current density, which can cause dendrite growth.

2.5. OER catalytic effect on oxygen cathodes

The VP additive dissolved in the electrolyte is close not only to the Li metal anode but also to the oxygen cathode part in a Li-O_2 cell. Therefore, to investigate the effects of the VP additive on the Li-O_2 reaction on the oxygen electrode, we conducted Li-O_2 cell tests employing the VP-containing electrolyte. Fig. 6 shows the electrochemical results for the cells. No significant reaction features were observed in the cyclic voltammetry (CV) curve under an inert (Ar purging) atmosphere (**Fig. S5**). However, after purging O_2, dominant peaks appeared in both the cathodic and anodic regions. The CV results for the Li-O_2 cells with the VP additive under the O_2 purging are shown in Fig. 5**a**. Typical CV peaks were observed in both the cathodic and anodic regions near 2.4 and 3.3 V, respectively. These peaks are associated with the typical formation and decomposition of Li_2O_2 products for discharging and charging ($2Li^+ + O_2 + 2e^- \leftrightarrow Li_2O_2$) [63]. While no additional peaks appeared for the electrolyte without VP, an additional peak was observed at 4.0 V after the addition of the VP additive. This additional anodic peak was attributed to a more effective OER owing to the VP additive. This result demonstrated that the VP worked not only as a stabilizing agent on the Li metal anode but also as a soluble electrolyte catalyst on the oxygen cathode. For Li-O_2 cells, the discharge product also inhibits charge transfer and causes a large overpotential for the OER because of its low conductivity [64]. To measure the degree of overpotential for the OER, we present galvanostatic intermittent titration test (GITT) curves obtained during the 10th charge cycle (Fig. 5**b**). Although the overpotential degrees ($\Delta V = 0.8$ V) at the mid-point were similar during the charging process, the cell containing VP exhibited a significantly lower charge voltage for the GITT testing time of 60 h than the cell without VP. At the end of charging, the overpotential degree in the VP-containing Li-O_2 cell was lower than that of the cell without VP. This result indicated that internal deterioration occurred during overcharging without the VP additive in the Li-O_2 cell. Although the electrolyte was vulnerable to decomposition as a result of the high voltage during overcharging, the VP could effectively suppress the decomposition of the electrolyte, thereby maintaining a stable charge overpotential. We evaluated the charge–discharge cycle test to further verify the beneficial effect of the VP additive (Fig. 5**c–f**). Fig. 5**c** presents the first charge/discharge profiles of MWCNT electrodes collected between 4.5 and 2.3 V at a current density of 100 mA g^{-1} in the LiTFSI + TEGDME electrolyte with and without VP. We observed a significantly lower voltage profile for the cell with the VP additive in the charging region, compared to that of the pristine Li-O_2 cell. This result corresponded to the CV result related to the anodic peak intensity increase, which indicated the catalytic effect of VP on the OER process. The lower charge potential correlated with the facile decomposition of discharge products promoted by the VP additive. We also show the cycle stability of the cells with and without VP (Fig. 5**d**). Consistent with the previous results, VP effectively worked as an OER catalyst in the electrolyte. In the case of the electrolyte without VP, the discharge capacity abruptly started to degrade after the 25th cycle, and cell operation ended after the 32nd cycle. Otherwise, Li-O_2 cell with VP maintained stable capacity without any degradation and started to decrease after the 50 cycles, indicating VP can also effectively work as stabilizer in Li-O_2 full cell. In addition, the terminal charge voltage rapidly reached the top of the voltage window of 4.5 V after the 10th cycle (Fig. 5**e**). In contrast, a cell with the VP additive exhibited a stable cycling performance with a consistent capacity value of 600 mAh g^{-1}_{carbon}. While a gradual decrease in the overpotential in the charge profiles for cycling was observed in the pristine cell as the cycle was repeated, a cell with the VP additive exhibited stable discharge voltage curves for repeated cycles (Fig. 5**f**). The electrochemical performances of the Li-O_2 cell in the presence/absence of the VP additive verified that the VP provided dual functions as both a soluble catalyst for Li-O_2 cells and surface stabilizing leveler for the Li metal anode. We reconfirmed the surface morphologies of the MWCNT electrodes at different electrochemical states (**Fig. S6**). After discharge, the discharge products were precipitated and clogged the surface of the electrode. The products were reversibly decomposed after the following charge process. There were no XRD peaks for the lithium oxide species or any other products for the discharged and charged electrodes, which showed that the products were formed as an amorphous phase rather than a crystalline structure (**Fig. S7**). The *ex-situ* characterization of the discharge products showed that the VP additive did not affect the formation of discharge products.

Fig. 6 schematically shows the roles of VP in both the anode and cathode. During lithium plating, electrons gather at the anode, and these electrons are concentrated in the protruding portion. Without VP, positively charged Li^+ ions gather in the protruding part with a high charge density and inhomogeneous distribution, causing dendrite growth. In addition, the oxide-based SEI layer easily cracks as a result of

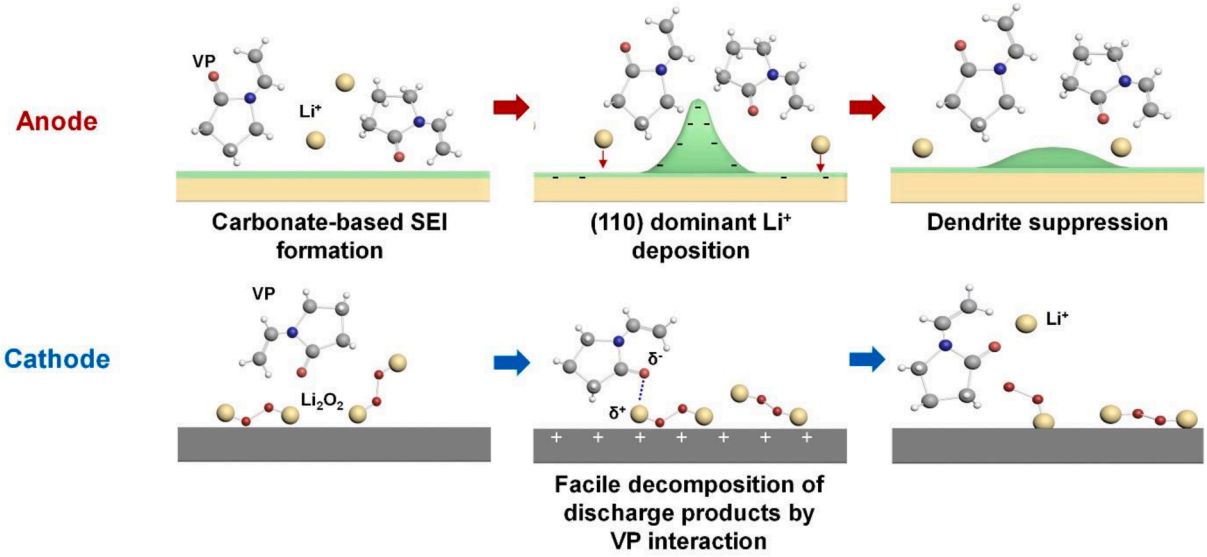

Fig. 6. Schematic illustration of dual-function mechanisms of the VP electrolyte additive on the anode and cathode of LMOBs.

the volume change in the Li, which leads to additional dendrite growth and dead Li accumulation. However, with VP, the LiF-containing carbonate-based SEI layer helps Li^+ ions diffuse and form a flexible and stable protective film. Because VP has a charge distribution in the molecule, the positively charged portion of VP is competitively collected in the protruding part of the Li anode, which prevents the reduction of Li^+ ions. During this deposition process, a (1 1 0) dominated surface forms a relatively uniform and excellent Li film. As a result, Li^+ ions are platinized in the part where the VP is not concentrated, and leveling occurs to minimize the overall curvature. In the cathode, VP exhibits an OER catalyst effect that assists in the decomposition of Li_2O_2. Because the cathode shows a positive charge during charging, VP is adsorbed to the surface in the direction of C═O bonding, which has a relatively negative charge. The oxygen of VP interacts with the Li, which has a positive charge of Li_2O_2, thereby weakening the Li-O bond in Li_2O_2. As a result, Li_2O_2 is decomposed more easily because of the relatively weakened Li-O bonding, decreasing the overpotential and enabling an increase in the number of cycles.

We showed that a VP additive could effectively level and rearrange a Li metal anode, stabilizing the electrolyte decomposition over 1000 cycles. We also successfully confirmed the effective catalytic reaction in a cathode. This suggests the possibility of a perfect RM for a safe and high-performance Li-O_2 battery system without the decomposition of the Li anode.

3. Conclusion

We demonstrated that a novel and dipolar VP electrolyte additive could exhibit dual functions by acting as a Li metal anode surface leveler and soluble cathode catalyst for low-resistance and long-cycling LMOBs. Li-Li symmetric cells with a VP-containing electrolyte exhibited significantly improved cycling performances with a reduced and stabilized overpotential even after 1200 cycles at high applied currents compared with those of pristine cells (<500 cycles). Reduced charge transfer resistance and ohmic resistance for cycling were also achieved by introducing the VP electrolyte additive. We directly confirmed that VP effectively suppressed dendrite growth through a surface leveling effect using diverse *ex-situ* morphological observation tools, such as cross-sectional SEM and AFM. We also confirmed through DFT calculations that the VP was effectively adsorbed on the Li surface, rendering a uniform Li surface. It was verified that the VP surrounding a Li metal anode surface chemically transformed an irregular LiOH impurity-rich SEI layer into a smooth and high-quality carbonate-rich film, which hindered dendrite growth and protected the Li metal surface from irreversible TEGDME decomposition. Significantly, the VP also functioned as an OER catalyst for facilitating a Li-O_2 cell reaction with reduced overpotential and longer cycle performance compared to the control. This study offered a novel direction to develop multi-functional and accessible electrolyte additives as anode surface stabilizers and soluble cathode catalysts to realize high-performance LMOBs.

4. Experimental section

4.1. Materials and chemicals

1-Vinyl-2-pyrrolidone (VP, 99 %), bis(trifluoromethane)sulfonimide lithium salt (LiTFSI, 99.95 %), tetraethylene glycol dimethyl ether (TEGDME, 99 %), poly(vinylidene fluoride) (PVDF, Mw ~ 180,000) and 1-methyl-2-pyrrolidone (NMP, anhydrous, 99.5 %) were purchased from Sigma-Aldrich (Korea). We used TEGDME after drying for several days and dipping freshly activated molecular sieves (type 4Å).

4.2. Preparation of Li-Li symmetric cells

A 12-mm diameter Li metal foil was used on both sides of the electrodes and a Celgard 2500 polypropylene (PP) separator was used. First, 1 M LiTFSI in TEGDME with 100 ppm VP was stirred for 24 h at room temperature. Electrolyte without VP was also produced to confirm the VP's effect on Li stripping/deposition. All the Li-Li symmetric cells were assembled into R2032 coin-type cells (Wellcos Corp.) in an argon-purged glovebox.

4.3. Preparation of Li – O_2 cells

An air-electrode was fabricated with 90 wt% MWCNT and 10 wt% PVDF dissolved in an NMP solution. This slurry was pasted onto a Ni-foam (MTI Korea, 13 mm in diameter) current collector and dried for 12 h in vacuum at 80 ℃. A 12-mm diameter Li metal foil was used as the anode, and glass fiber (Whatman GF/A microfiber filter paper) was used as the separator. The prepared air electrode was assembled in sequence in an HS air-type cell (HS flat cell combined with Swagelok type, EK cell, Wellcos Corp.) in an Ar-filled glove box. All the cells were assembled into R2032 coin-type cells with several holes (Wellcos Corp.).

4.4. Ex-situ characterizations

The surface characterizations of the electrodes after cycling were conducted using XPS (K-alpha, Thermo U.K.) and XRD (D8 Advance, Bruker) using Cu-Kα (λ = 1.54 Å) radiation. The surface morphologies were observed using a field emission SEM (FE-SEM, JSM-7600F, JEOL). The surface roughness was investigated using AFM (NX-10, Park Systems Korea) in the glove box. The samples were prepared via galvanostatic discharging and charging. Pristine electrodes were dipped in the electrolyte to compare each sample. Cells were disassembled in an Ar-filled glove box after the cycle test. The collected electrodes were dried in a vacuum chamber over 12 h to remove the electrolyte.

4.5. Electrochemical characterization

The charge/discharge tests were conducted using a potentiogalvanostat cycler (WBCS3000S battery test system, WonATech). Li-O_2 cells were tested at a current density of 100 mA g^{-1} in a voltage range of 2.3–4.5 V vs Li/Li^+. A Biologic VSP potentiostat with an impedance function was used for CV experiments, GITT, and EIS measurements of the cells. All the electrochemical experiments were conducted at room temperature.

4.6. Computational details

GGA-level, spin-polarized DFT calculations were performed with the Vienna ab-initio simulation package using a plane-wave basis set with a cut-off energy of 400 eV. The Revised Perdew-Burke-Ernzerhof (RPBE) functional was used to describe the electron exchange and correlation [65–67]. The Brillouin zone was sampled at 2 × 2 × 1 based on the Monkhost-Pack scheme. The convergence criteria for the electronic and geometric optimizations were 10^{-5} eV and 10^{-2} eV/Å, respectively. The (1 1 0) surfaces had the lowest surface energies among the various surfaces of the body centered cubic (BCC) Li bulk [68]. Even though the (1 1 0) surface was the most stable, the actual surface of the Li anode should have defects and steps that can cause the Li dendrite formation. Therefore, we made the (1 1 0) surface with a step to consider different kinds of binding sites, which had a 20 Å vacuum gap in the z-direction. Two bottom layers were fixed in the bulk position among the four atomic layers. To calculate the binding energy of the Li or VP additive, the following equation was used.

$$\Delta E_{bind} = \Delta E_{Surface+Li(orVP)} - \Delta E_{surface} - \Delta E_{Li(orVP)}$$

Here, ΔE_{bind} is the binding energy of the adsorbate; $\Delta E_{Surface+Li(orVP)}$ is the total energy of the system, including the surface and adsorbate; $\Delta E_{surface}$ is the total energy of the isolated surface; $\Delta E_{Li(orVP)}$ is the bulk cohesive energy of Li or gas phase energy of the VP additive.

Declaration of Competing Interest

The authors declare that they have no known competing financial interests or personal relationships that could have appeared to influence the work reported in this paper.

Data availability

Data will be made available on request.

Acknowledgments

This study was supported by the National Research Foundation of Korea (NRF) grant funded by the Korean government (MSIT) (Nos. 2018R1A5A1025224). This study was also supported by the KIST Institutional Program (Project No. 2E31861). This work was partly supported by the Korea Institute of Energy Technology Evaluation and Planning (KETEP) grant funded by the Korean government (MOTIE) (20221B1010003B, Integrated High-Quality Technology Development of Remanufacturing Spent Cathode for Low Carbon Resource Recirculation).

Appendix A. Supplementary data

Supplementary data to this article can be found online at https://doi.org/10.1016/j.cej.2023.141383.

References

[1] S. Chu, Y. Cui, N. Liu, The path towards sustainable energy, Nat. Mater. 16 (1) (2017) 16–22.
[2] J.B. Goodenough, K.S. Park, The Li-Ion Rechargeable Battery: A Perspective, J. Am. Chem. Soc. 135 (4) (2013) 1167–1176.
[3] O. Schmidt, A. Hawkes, A. Gambhir, I. Staffell, The future cost of electrical energy storage based on experience rates, Nat. Energy 2 (8) (2017).
[4] J.W. Jung, C.L. Lee, S. Yu, I.D. Kim, Electrospun nanofibers as a platform for advanced secondary batteries: a comprehensive review, J. Mater. Chem. A 4 (3) (2016) 703–750.
[5] J.W. Choi, D. Aurbach, Promise and reality of post-lithium-ion batteries with high energy densities, Nat. Rev. Mater. 1 (4) (2016).
[6] L.C. Yue, C. Ma, S.A. Yan, Z.G. Wu, W.X. Zhao, Q. Liu, Y.L. Luo, B.H. Zhong, F. Zhang, Y. Liu, A.A. Alshehri, K.A. Alzahrani, X.D. Guo, X.P. Sun, Improving the intrinsic electronic conductivity of NiMoO4 anodes by phosphorous doping for high lithium storage, Nano Res. 15 (1) (2022) 186–194.
[7] W. Xu, J.L. Wang, F. Ding, X.L. Chen, E. Nasybutin, Y.H. Zhang, J.G. Zhang, Lithium metal anodes for rechargeable batteries, Energ. Environ. Sci. 7 (2) (2014) 513–537.
[8] D.C. Lin, Y.Y. Liu, Y. Cui, Reviving the lithium metal anode for high-energy batteries, Nat. Nanotechnol. 12 (3) (2017) 194–206.
[9] X. Shen, H. Liu, X.B. Cheng, C. Yan, J.Q. Huang, Beyond lithium ion batteries: Higher energy density battery systems based on lithium metal anodes, Energy Storage Mater. 12 (2018) 161–175.
[10] P.C. Zou, Y. Wang, S.W. Chiang, X.Y. Wang, F.Y. Kang, C. Yang, Directing lateral growth of lithium dendrites in micro-compartmented anode arrays for safe lithium metal batteries, Nat. Commun. 9 (2018).
[11] L. Yue, D. Wang, Z. Wu, W. Zhao, Y. Ren, L. Zhang, B. Zhong, N.a. Li, B.o. Tang, Q. Liu, Y. Luo, A.M. Asiri, X. Guo, X. Sun, Polyrrole-encapsulated Cu2Se nanosheets in situ grown on Cu mesh for high stability sodium-ion battery anode, Chem. Eng. J. 433 (2022) 134477.
[12] H. Qiu, T. Tang, M. Asif, X. Huang, Y. Hou, 3D Porous Cu Current Collectors Derived by Hydrogen Bubble Dynamic Template for Enhanced Li Metal Anode Performance, Adv. Funct. Mater. 29 (19) (2019) 1808468.
[13] H. Liu, E.R. Wang, Q. Zhang, Y.B. Ren, X.W. Guo, L. Wang, G.Y. Li, H.J. Yu, Unique 3D nanoporous/macroporous structure Cu current collector for dendrite-free lithium deposition, Energy Storage Mater. 17 (2019) 253–259.
[14] S. Matsuda, Y. Kubo, K. Uosaki, S. Nakanishi, Insulative Microfiber 3D Matrix as a Host Material Minimizing Volume Change of the Anode of Li Metal Batteries, ACS Energy Lett. 2 (4) (2017) 924–929.
[15] H. Lee, J. Song, Y.J. Kim, J.K. Park, H.T. Kim, Structural modulation of lithium metal-electrolyte interface with three-dimensional metallic interlayer for high-performance lithium metal batteries, Sci. Rep-Uk 6 (2016).
[16] X.B. Cheng, M.Q. Zhao, C. Chen, A. Pentecost, K. Maleski, T. Mathis, X.Q. Zhang, Q. Zhang, J.J. Jiang, Y. Gogotsi, Nanodiamonds suppress the growth of lithium dendrites, Nat. Commun. 8 (2017).
[17] Q. Wang, C. Yang, J. Yang, K. Wu, C. Hu, J. Lu, W. Liu, X. Sun, J. Qiu, H. Zhou, Dendrite-Free Lithium Deposition via a Superfilling Mechanism for High-Performance Li-Metal Batteries, Adv. Mater. 31 (41) (2019) 1903248.
[18] G.X. Lu, J.W. Nai, H.D. Yuan, J.C. Wang, J.H. Zheng, Z.J. Ju, C.B. Jin, Y. Wang, T. F. Liu, Y.J. Liu, X.Y. Tao, In-Situ Electrodeposition of Nanostructured Carbon Strengthened Interface for Stabilizing Lithium Metal Anode, ACS Nano 16 (6) (2022) 9883–9893.
[19] O.W. Sheng, C.B. Jin, Z.J. Ju, J.H. Zheng, T.F. Liu, Y.J. Liu, Y. Wang, J.M. Luo, X. Y. Tao, J.W. Nai, Stabilizing Li4SnS4 Electrolyte from Interface to Bulk Phase with a Gradient Lithium in Lithium Metal Batteries, Nano Lett (2022).
[20] H.D. Yuan, J.W. Nai, H. Tian, Z.J. Ju, W.K. Zhang, Y.J. Liu, X.Y. Tao, X.W. Lou, An ultrastable lithium metal anode enabled by designed metal fluoride spansules, Sci. Adv. 6 (10) (2020).
[21] L.C. Yue, J. Liang, Z.G. Wu, B.H. Zhong, Y.L. Luo, Q. Liu, T.S. Li, Q.Q. Kong, Y. Liu, A.M. Asiri, X.D. Guo, X.P. Sun, Progress and perspective of metal phosphide/carbon heterostructure anodes for rechargeable ion batteries, J. Mater. Chem. A 9 (20) (2021) 11879–11907.
[22] P.G. Bruce, S.A. Freunberger, L.J. Hardwick, J.M. Tarascon, Li-O-2 and Li-S batteries with high energy storage, Nat. Mater. 11 (1) (2012) 19–29.
[23] Y.J. Rho, B. Kim, K. Shin, G. Henkelman, W.H. Ryu, Atomically miniaturized bi-phase IrOx/Ir catalysts loaded on N-doped carbon nanotubes for high-performance Li-CO2 batteries, J. Mater. Chem. A 10 (37) (2022) 19710–19721.
[24] H.S. Kim, J.Y. Lee, J.K. Yoo, W.H. Ryu, Capillary-Driven Formation of Iron Nanoparticles Embedded in Nanotubes for Catalyzed Lithium-Carbon Dioxide Reaction, ACS Mater. Lett. 3 (6) (2021) 815–825.
[25] J. Lu, Y. Jung Lee, X. Luo, K. Chun Lau, M. Asadi, H.-H. Wang, S. Brombosz, J. Wen, D. Zhai, Z. Chen, D.J. Miller, Y.o. Sub Jeong, J.-B. Park, Z. Zak Fang, B. Kumar, A. Salehi-Khojin, Y.-K. Sun, L.A. Curtiss, K. Amine, A lithium-oxygen battery based on lithium superoxide, Nature 529 (7586) (2016) 377–382.
[26] W.H. Ryu, T.H. Yoon, S.H. Song, S. Jeon, Y.J. Park, I.D. Kim, Bifunctional Composite Catalysts Using Co3O4 Nanofibers Immobilized on Nonoxidized Graphene Nanoflakes for High-Capacity and Long-Cycle Li-O-2 Batteries, Nano Lett. 13 (9) (2013) 4190–4197.
[27] X.H. Yao, Q. Dong, Q.M. Cheng, D.W. Wang, Why Do Lithium-Oxygen Batteries Fail: Parasitic Chemical Reactions and Their Synergistic Effect, Angew. Chem. Int. Edit. 55 (38) (2016) 11344–11353.
[28] G.-Y. Kim, J. Lee, Y.-J. Rho, W.-H. Kim, MinJoong Kim, J.-H. Ahn, W.-H. Ryu, Rhenium oxide/sulfide binary phase flakes decorated on nanofiber support for enhanced activation of electrochemical conversion reactions, Chem. Eng. J. 446 (2022) 136951.
[29] G.-Y. Kim, K.R. Yoon, K. Shin, J.-W. Jung, G. Henkelman, W.-H. Ryu, Black Tungsten Oxide Nanofiber as a Robust Support for Metal Catalysts: High Catalyst Loading for Electrochemical Oxygen Reduction, Small 17 (47) (2021) 2103755.
[30] W.H. Ryu, F.S. Gittleson, M. Schwab, T. Goh, A.D. Taylor, A Mesoporous Catalytic Membrane Architecture for Lithium-Oxygen Battery Systems, Nano Lett. 15 (1) (2015) 434–441.
[31] W.H. Ryu, F.S. Gittleson, J.Y. Li, X. Tong, A.D. Taylor, A New Design Strategy for Observing Lithium Oxide Growth-Evolution Interactions Using Geometric Catalyst Positioning, Nano Lett. 16 (8) (2016) 4799–4806.
[32] K.R. Yoon, D.S. Kim, W.H. Ryu, S.H. Song, D.Y. Youn, J.W. Jung, S. Jeon, Y.J. Park, I.D. Kim, Tailored Combination of Low Dimensional Catalysts for Efficient Oxygen Reduction and Evolution in Li-O-2 Batteries, Chemsuschem 9 (16) (2016) 2080–2088.
[33] J.S. Lee, C. Lee, J.Y. Lee, J. Ryu, W.H. Ryu, Polyoxometalate as a Nature-Inspired Bifunctional Catalyst for Lithium-Oxygen Batteries, ACS Catal. 8 (8) (2018) 7213–7221.
[34] W.H. Ryu, F.S. Gittleson, J.M. Thomsen, J.Y. Li, M.J. Schwab, G.W. Brudvig, A. D. Taylor, Heme biomolecule as redox mediator and oxygen shuttle for efficient charging of lithium-oxygen batteries, Nat. Commun. 7 (2016).
[35] H.D. Lim, H. Song, J. Kim, H. Gwon, Y. Bae, K.Y. Park, J. Hong, H. Kim, T. Kim, Y. H. Kim, X. Lepro, R. Ovalle-Robles, R.H. Baughman, K. Kang, Superior Rechargeability and Efficiency of Lithium-Oxygen Batteries: Hierarchical Air Electrode Architecture Combined with a Soluble Catalyst, Angew. Chem. Int. Edit. 53 (15) (2014) 3926–3931.
[36] W.J. Kwak, D. Hirshberg, D. Sharon, M. Afri, A.A. Frimer, H.G. Jung, D. Aurbach, Y.K. Sun, Li-O-2 cells with LiBr as an electrolyte and a redox mediator, Energ. Environ. Sci. 9 (7) (2016) 2334–2345.
[37] J.-B. Park, S.H. Lee, H.-G. Jung, D. Aurbach, Y.-K. Sun, Redox Mediators for Li-O-2 Batteries: Status and Perspectives, Adv. Mater. 30 (1) (2018) 1704162.
[38] H.-S. Kim, B. Kim, H. Park, J. Kim, W.-H. Ryu, Auto-Oxygenated Porphyrin-Derived Redox Mediators for High-Performance Lithium Air-Breathing Batteries, Adv. Energy Mater. 12 (7) (2022) 2103527.
[39] H.S. Kim, B. Kim, H.D. Lim, W.H. Ryu, Self-Oxygenated Blood Protein-Embedded Nanotube Catalysts forLonger Cyclable Lithium Oxygen-Breathing Batteries, ACS Sustain. Chem. Eng. 10 (13) (2022) 4198–4205.
[40] S. Ha, Y. Kim, D. Koo, K.H. Ha, Y. Park, D.M. Kim, S. Son, T. Yim, K.T. Lee, Investigation into the stability of Li metal anodes in Li-O-2 batteries with a redox mediator, J. Mater. Chem. A 5 (21) (2017) 10609–10621.
[41] D. Sun, Y. Shen, W. Zhang, L. Yu, Z.Q. Yi, W. Yin, D. Wang, Y.H. Huang, J. Wang, D.L. Wang, J.B. Goodenough, A Solution-Phase Bifunctional Catalyst for Lithium-Oxygen Batteries, J. Am. Chem. Soc. 136 (25) (2014) 8941–8946.
[42] N.T.M. Hai, J. Furrer, F. Stricker, T.M.T. Huynh, I. Gjuroski, N. Luedi, T. Brunner, F. Weiss, A. Fluegel, M. Arnold, I. Chang, D. Mayer, P. Broekmann, Polyvinylpyrrolidones (PVPs): Switchable Leveler Additives for Damascene Applications, J. Electrochem. Soc. 160 (12) (2013) D3116–D3125.
[43] M.J. Willey, J. Reid, A.C. West, Adsorption kinetics of polyvinylpyrrolidone during copper electrodeposition, Electrochem. Solid St. 10 (4) (2007) D38–D41.

[44] S.H. Jin, Y. Yoon, Y. Jo, S. Lee, H. Moon, S. Seok, M.J. Kim, J.J. Kim, M.H. Lee, The effects of polyvinylpyrrolidone molecular weight on defect-free filling of through-glass vias (TGVs), J. Ind. Eng. Chem. 96 (2021) 376–381.
[45] K.N. Wood, M. Noked, N.P. Dasgupta, Lithium metal anodes: toward an improved understanding of coupled morphological, electrochemical, and mechanical behavior, ACS Energy Lett. 2 (3) (2017) 664–672.
[46] K.N. Wood, E. Kazyak, A.F. Chadwick, K.-H. Chen, J.-G. Zhang, K. Thornton, N.P. Dasgupta, Dendrites and Pits: Untangling the Complex Behavior of Li Metal Anodes through Operando Video Microscopy, ECS Meeting Abstracts, IOP Publishing, 2017, p. 518.
[47] K.H. Chen, K.N. Wood, E. Kazyak, W.S. LePage, A.L. Davis, A.J. Sanchez, N. P. Dasgupta, Dead lithium: mass transport effects on voltage, capacity, and failure of lithium metal anodes, J. Mater. Chem. A 5 (23) (2017) 11671–11681.
[48] K.N. Wood, E. Kazyak, A.F. Chadwick, K.H. Chen, J.G. Zhang, K. Thornton, N. P. Dasgupta, Dendrites and Pits: Untangling the Complex Behavior of Lithium Metal Anodes through Operando Video Microscopy, ACS Central. Sci. 2 (11) (2016) 790–801.
[49] L. Frenck, G.K. Sethi, J.A. Maslyn, N.P. Balsara, Factors That Control the Formation of Dendrites and Other Morphologies on Lithium Metal Anodes, Front. Energy Res. 7 (2019).
[50] W. Choi, H.C. Shin, J.M. Kim, J.Y. Choi, W.S. Yoon, Modeling and Applications of Electrochemical Impedance Spectroscopy (EIS) for Lithium-ion Batteries, J. Electrochem. Sci. Te. 11 (1) (2020) 1–13.
[51] Z.L. Hu, S. Zhang, S.M. Dong, Q. Li, G.L. Cui, L.Q. Chen, Self-Stabilized Solid Electrolyte Interface on a Host-Free Li-Metal Anode toward High Areal Capacity and Rate Utilization, Chem. Mater. 30 (12) (2018) 4039–4047.
[52] T. Liu, M. Leskes, W.J. Yu, A.J. Moore, L.N. Zhou, P.M. Bayley, G. Kim, C.P. Grey, Cycling Li-O-2 batteries via LiOH formation and decomposition, Science 350 (6260) (2015) 530–533.
[53] G. Karkera, A.S. Prakash, Decoupling the Cumulative Contributions of Capacity Fade in Ethereal-Based Li-O-2 Batteries, ACS Appl. Mater. Inter. 11 (31) (2019) 27870–27881.
[54] F. Shi, A. Pei, A. Vailionis, J. Xie, B. Liu, J. Zhao, Y. Gong, Y. Cui, Strong texturing of lithium metal in batteries, Proc. Natl. Acad. Sci. U. S. A. 114 (46) (2017) 12138–12143.
[55] Q. Zhao, Y. Deng, N.W. Utomo, J. Zheng, P. Biswal, J. Yin, L.A. Archer, On the crystallography and reversibility of lithium electrodeposits at ultrahigh capacity, Nat. Commun. 12 (1) (2021) 1–10.
[56] M.F. He, R. Guo, G.M. Hobold, H.N. Gao, B.M. Gallant, The intrinsic behavior of lithium fluoride in solid electrolyte interphases on lithium, Proc. Natl. Acad. Sci. U. S. A. 117 (1) (2020) 73–79.
[57] X.-Q. Zhang, X.-B. Cheng, X. Chen, C. Yan, Q. Zhang, Fluoroethylene Carbonate Additives to Render Uniform Li Deposits in Lithium Metal Batteries, Adv. Funct. Mater. 27 (10) (2017) 1605989.
[58] J.D. McBrayer, C.A. Apblett, K.L. Harrison, K.R. Fenton, S.D. Minteer, Mechanical studies of the solid electrolyte interphase on anodes in lithium and lithium ion batteries, Nanotechnology 32 (50) (2021) 502005.
[59] U.v. Alpen,, Li3N: A promising Li ionic conductor, Journal of Solid State Chemistry 29 (3) (1979) 379–392.
[60] Y. Zhang, W. Wang, H. Tang, W. Bai, X. Ge, X. Wang, C. Gu, J.P. Tu, An ex-situ nitridation route to synthesize Li3N-modified Li anodes for lithium secondary batteries, J. Power Sources 277 (2015) 304–311.
[61] A.Y. Wang, B. Chen, L. Fang, J.J. Yu, L.M. Wang, Influence of branched quaternary ammonium surfactant molecules as levelers for copper electroplating from acidic sulfate bath, Electrochim. Acta 108 (2013) 698–706.
[62] F. Ding, W. Xu, G.L. Graff, J. Zhang, M.L. Sushko, X.L. Chen, Y.Y. Shao, M. H. Engelhard, Z.M. Nie, J. Xiao, X.J. Liu, P.V. Sushko, J. Liu, J.G. Zhang, Dendrite-Free Lithium Deposition via Self-Healing Electrostatic Shield Mechanism, J. Am. Chem. Soc. 135 (11) (2013) 4450–4456.
[63] F.S. Gittleson, R.E. Jones, D.K. Ward, M.E. Foster, Oxygen solubility and transport in Li-air battery electrolytes: establishing criteria and strategies for electrolyte design, Energ. Environ. Sci. 10 (5) (2017) 1167–1179.
[64] V. Viswanathan, K.S. Thygesen, J.S. Hummelshøj, J.K. Nørskov, G. Girishkumar, B. D. McCloskey, A.C. Luntz, Electrical conductivity in Li2O2 and its role in determining capacity limitations in non-aqueous Li-O-2 batteries, J. Chem. Phys. 135 (21) (2011) 214704.
[65] J.P. Perdew, K. Burke, M. Ernzerhof, Generalized Gradient Approximation Made Simple, Physical Review Letters 77 (18) (1996) 3865–3868.
[66] Y. Zhang, W. Yang, Comment on "Generalized Gradient Approximation Made Simple'', Physical Review Letters 80 (4) (1998) 890-890.
[67] B. Hammer, L.B. Hansen, J.K. Nørskov, Improved adsorption energetics within density-functional theory using revised Perdew-Burke-Ernzerhof functionals, Physical Review B 59 (11) (1999) 7413–7421.
[68] J.M. Zhang, F. Ma, K.W. Xu, Calculation of the surface energy of bcc metals by using the modified embedded-atom method, Surface Interface Anal. 35 (8) (2003) 662–666.